First-principles study of the dipole layer formation at metal-organic interfaces

Paul C. Rusu,[1] Gianluca Giovannetti,[2] Christ Weijtens,[3] Reinder Coehoorn,[4] and Geert Brocks[1]

[1]*Computational Materials Science, Faculty of Science and Technology and MESA+ Institute for Nanotechnology, University of Twente, P.O. Box 217, 7500 AE Enschede, The Netherlands*

[2]*CASTI Regional Laboratory, Consiglio Nazionale delle Ricerche-Istituto Nazionale per la Fisica della Materia (CNR-INFM), 67100 L'Aquila, Italy*

[3]*Philips Research Laboratories Aachen, Weisshausstrasse 2, D-52066 Aachen, Germany*

[4]*Philips Research Laboratories, Prof. Holstlaan 4, 5656 AA Eindhoven, The Netherlands*

(Received 23 July 2009; revised manuscript received 15 January 2010; published 3 March 2010)

We study the dipole layer formed at metal-organic interfaces by means of first-principles calculations. Interface dipoles are monitored by calculating the change in the work-function of Au, Ag, Al, Mg, and Ca surfaces upon adsorption of a monolayer of 3,4,9,10-perylene-tetra-carboxylic-di-anhydride (PTCDA), perylene, or benzene molecules. Adsorption of PTCDA leads to pinning of the work function for a range of metal substrates. It gives interface dipoles that compensate for the difference in the clean metal work functions, leading to a nearly constant work function. In contrast, adsorption of benzene always results in a decrease in the work function, which is relatively constant for all metal substrates. Both effects are found in perylene, where adsorption on low-work-function metals gives work-function pinning, whereas adsorption on high-work-function metals gives work-function lowering. The work function changes upon adsorption are analyzed and interpreted in terms of two competing effects. If the molecule and substrate interact weakly, the molecule pushes electrons into the surface, which lowers the work function. If the metal work function is sufficiently low with respect to the unoccupied states of the molecule, electrons are donated into these states, which increases the binding and the work function.

DOI: 10.1103/PhysRevB.81.125403 PACS number(s): 73.30.+y, 73.61.Ph, 68.43.−h

I. INTRODUCTION

Applications of organic semiconductors in light-emitting diodes,[1,2] field-effect transistors,[3,4] and solar cells[5,6] have stimulated research into the fundamental electronic properties of organic materials and their interfaces with metal electrodes.[7,8] The weak forces between the molecules in an organic material lead to small band widths, which enhances the importance of electron-phonon and electron-electron interactions.[9–12] Nevertheless high charge-carrier mobilities can be achieved in well-ordered molecular crystals.[7] As the quality of molecular crystals increases, transport of charge carriers across the interfaces between metal electrodes and the organic material starts to determine the performance of the devices.[13] Metal-organic interfaces (MOIs) often give rise to a non-Ohmic behavior, indicating the existence of significant Schottky barriers.

Chemical bonding between molecules and metal surfaces modifies the charge distribution at a MOI. It results in an interface dipole layer, which strongly influences the Schottky barrier height.[14–16] This effect of chemical bonding is observed very clearly in self-assembled monolayers (SAMs) of thiolate molecules chemically bonded to noble metal surfaces.[16–21] Common organic semiconductors, however, consist of closed shell molecules, which are usually thought to bind weakly to metal surfaces. It has therefore been assumed for a long time that the charge reordering at such MOIs is insignificant and that no appreciable interface dipole is formed.

In absence of an interface dipole, the Schottky barrier at a MOI can be predicted by aligning the vacuum levels of the metal and the organic material, called the Schottky-Mott rule. Over the last decade, however, experimental studies have indicated the general breakdown of the vacuum alignment rule and have demonstrated that significant interface dipoles are formed at MOIs.[8,22–26] In addition such studies have shown that interface dipoles at MOIs are localized foremost at the first molecular layer covering the metal. The interface dipoles are not affected much by deposition of additional organic layers. Because MOI dipoles are localized at the interface, they can be extracted from the change in the surface work function after deposition of a single organic layer.

Ideas inspired by chemical bonding have been put forward to explain large interface dipoles. Conventional semiconductors such as Si have reactive surfaces, which bind strongly to metal overlayers. A significant density of states is then often created at the metal-semiconductor interface within the band gap of the semiconductor, the so-called metal-induced gap states (MIGS).[27–29] In this model, MIGS determine the charge distribution at the interface and hence the interface dipole. The MIGS model has also been applied to MOIs.[30–32] It requires a strong interaction between the metal and the organic material.

If molecules are physisorbed onto a metal surface, one expects a relatively weak interaction between the molecular semiconductor and the metal. For physisorbed molecules interface dipoles at MOIs have been explained by the so-called pillow effect.[33–37] Pauli exchange repulsion pushes electrons back into the metal, which yields an interface dipole that decreases the surface work function.

A decrease in the work function is commonly found if inert atoms or small molecules are adsorbed on a metal surface.[33–38] Remarkably, adsorption of larger, π conjugated, molecules can lead to a substantial increase, as well as a

decrease in the work function and the dependence of this work-function shift and the associated interface dipole on the molecules and the metal has been the subject of intensive experimental study.[8,22–26] If the work function W of a surface after coverage with a molecular layer is measured for a range of metal substrates with different initial work functions W_c, the results can be characterized by the parameter

$$S = \frac{dW}{dW_c}, \tag{1}$$

where W_c and W are the work functions of the clean metal surface and of the surface with the adsorbed organic layer, respectively.

The vacuum-level alignment, or Schottky-Mott rule gives $S=1$. Assuming that the pillow effect does not depend strongly on the metal substrate, it gives a relatively constant decrease in the work function, leading to $S \approx 1$. Although this is observed for some molecules, very often S is significantly smaller than 1.[8] Moreover, there is no *a priori* reason why S should be a constant. Indeed for some molecules and polymers several regimes can be distinguished, between which a transition from $S \approx 1$ to $S \approx 0$ is observed.[39–42] For the case where the organic layer is separated from the metal electrode by a thin insulating barrier, this behavior is interpreted with a model that assumes charge transfer across this barrier.[43–45]

In this paper we study the dipole formation at interfaces of monolayers of 3,4,9,10-perylene-tetra-carboxylic-dianhydride (PTCDA), perylene, and benzene molecules adsorbed on close-packed metal surfaces of Au, Ag, Al, Mg, and Ca by means of density-functional theory (DFT) calculations. We have selected these surfaces because they have a similar and simple structure, as well as a simple electronic (free-electronlike) structure. Yet their work functions span a range from 3.0 eV (Ca) to 5.3 eV (Au), allowing to study the effect of the metal work function on the interface dipole. A preliminary account of this work has been given in Ref. 46.

The molecules are chosen on account of their difference in complexity and their different behavior experimentally. PTCDA is a fairly complex conjugated molecule with a relatively small electronic gap. From an experimental point of view a PTCDA monolayer on metal surfaces has been a model system to study MOIs. Deposition of PTCDA on noble metal surfaces leads to well-ordered epitaxial overlayers.[47] In particular the structure and electronic structure of PTCDA on Ag(111) have been studied intensively.[48–56] Work-function measurements have been performed for PTCDA adsorbed on a range of metal surfaces.[8,22,57,58] These measurements give a work function that is roughly independent of the metal substrate, i.e., $S \approx 0$, meaning that adsorption of a PTCDA monolayer on a high work-function metal gives a decrease in the work function, whereas adsorption on a low work-function metal gives an increase.

In contrast, experimental data suggest that adsorption of the simple conjugated molecule benzene on a metal surface always gives a decrease in the work function, with S in the range 0.6–1.0.[37,59–63] The size and complexity of the perylene molecule is between that of benzene and PTCDA. The structure of an adsorbed perylene monolayer is thought to be similar to that of a PTCDA layer.[50,64,65] Depending on the metal substrate, the work function can decrease or increase, but there is no uniform pinning as for PTCDA.[66]

This paper is organized as follows. In the next section we give the technical details of our calculations. In Sec. III we present our results obtained for adsorption of PTCDA monolayers on different metal surfaces. We compare results obtained with different density functionals, and study the influence of the packing density of the molecules on the surface. Section IV gives the results obtained for adsorbed benzene and perylene monolayers. The results are discussed in Sec. V with the help of a simple phenomenological model, and a short summary and conclusions are given in Sec. VI.

II. COMPUTATIONAL DETAILS

The electronic structure is treated within DFT (Refs. 67 and 68) using the local-density approximation (LDA),[69,70] or the generalized gradient approximation (GGA) with the PW91 exchange-correlation functional.[71] The calculations are performed with the Vienna *ab initio* simulation package (VASP) program,[72,73] which uses the projector augmented wave method.[74,75] For Au and Ag atoms the outer shell d and s electrons are treated as valence electrons, for Al the outer shell s and p electrons, and for Mg and Ca the outer shell s electrons. For atoms of first row elements the $2s$ and $2p$ electrons are treated as valence electrons. The valence pseudowave functions are expanded in a basis set consisting of plane waves. All plane waves up to a kinetic-energy cutoff of 400 eV are included.

To model the metal-molecule interface, we use a supercell containing a slab of at least three metal layers with one layer of molecules adsorbed on one surface, and a vacuum region of at least 10 Å. Periodic boundary conditions are applied and the atomic positions in the top metal layer and in the molecules are allowed to relax. A dipole correction is applied to avoid spurious interactions between dipoles of repeated slabs along the direction normal to the surface.[76]

The electronic structure is calculated self-consistently using a 3×3 (for PTCDA) to 5×5 (for perylene and benzene) **k**-point grid in the surface Brillouin zone (SBZ) according to the Monkhorst-Pack scheme[77] and applying a Methfessel-Paxton smearing of 0.2 eV.[78] A 3×3 **k**-point grid gives well-converged results for PTCDA layers, because of the large size of the surface unit cell (see next section). The convergence criteria for electronic and structural optimization are set to 10^{-4} eV. For accurate calculations of total energies and densities of states (DOSs) the charge densities are recalculated with a 7×7 **k**-point grid, using the tetrahedron method.[79] DOSs are plotted using Gaussian smearing with a broadening parameter of 0.1 eV.

Work functions are evaluated from the expression

$$W = V(\infty) - E_F, \tag{2}$$

where $V(\infty)$ is the electrostatic potential in the vacuum region and E_F is the Fermi energy of the bulk metal. $V(\infty)$ is obtained from the potential averaged in the (x,y) plane

TABLE I. Optimized nearest-neighbor distances in the bulk metals. All values are in angstrom.

	Au	Ag	Al	Mg	Ca
GGA	2.94	2.93	2.86	3.19	3.92
LDA	2.87	2.84	2.82	3.13	3.78
Expt.	2.88	2.89	2.86	3.21	3.95

$$\bar{V}(z) = \frac{1}{A}\int\int_{cell} V(x,y,z)dxdy, \tag{3}$$

where $V(x,y,z)$ is the electrostatic potential on a real-space grid in the supercell. In practice $\bar{V}(z)$ reaches an asymptotic value $V(\infty)$ at a distance of a few angstrom from the surface.[19,21] An accurate value of E_F is obtained from a separate bulk calculation, following the procedure described in Ref. 80.

We have performed test calculations varying the number of metal layers used in the slab, the vacuum thickness, **k**-point sampling grid, and plane-waves kinetic-energy cutoff. From these tests we find that with the parameters given above, total energies are converged to within 0.01 eV and the work functions given in this paper to within 0.05 eV. The results for PTCDA on Ca(111) turn out to be the most sensitive with respect to vacuum thickness and **k**-point sampling. So for this system the results have been obtained using a 5×5 **k**-point grid in the SBZ and a vacuum thickness of at least 14 Å.

To analyze our results we also use properties of isolated molecules, such as the electron affinity (EA), as will be discussed in Sec. V. For calculations on isolated molecules we use the GAMESS program,[81] and treat the electronic structure within DFT using the BLYP functional.[82,83] We use the $6-31+G^*$ basis set, which gives EAs for acenes that are converged on a scale of ~0.1 eV.[84] As in Ref. 84, we find that including a diffuse orbital in the basis set is important and that the smaller $6-31G^*$ basis set does not give a sufficiently converged EA.[85] For instance, the EAs of PTCDA obtained using the $6-31G^*$ and $6-31+G^*$ bases differ by 0.4 eV. The Kohn-Sham (KS) energy levels of the (neutral) isolated molecule calculated with VASP and GAMESS are very similar, illustrating that, provided the basis sets are sufficiently converged, the PW91 and BLYP functionals give similar results.

III. PTCDA

Before discussing the results obtained for adsorbed layers, we benchmark our calculations on clean metal surfaces. We consider the close-packed (111) surfaces of fcc Au, Ag, Al, and Ca, and the (0001) surface of hcp Mg. The metals in this set are relatively simple, free electronlike and the set of surfaces spans a considerable range in work functions. Table I lists the optimized nearest-neighbor distances of the bulk metals, calculated with GGA(PW91) and LDA functionals. As usual, the GGA values are larger than the LDA values, but both are generally in reasonable agreement with experiment. We use these optimized distances to construct the surface unit cells.

Table II lists the calculated work functions of the clean (111) surfaces [for Mg the (0001) surface], compared to experimental values and values obtained in previous calculations. Our results have been obtained using slabs consisting of six metal layers. A 25×25 **k**-point sampling of the SBZ is applied, while allowing the top two metal layers to relax. The GGA values generally are within ~0.1 eV of the experimental values. LDA still gives an acceptable accuracy, but tends to overestimate the work function somewhat. Only for Al(111) LDA gives a better value than GGA, as compared to experiment. Our results also agree with those obtained in previous computational studies; the small differences can be attributed to differences in the computational parameters, such as the functional, the basis set, and the lattice parameter.

TABLE II. Calculated work functions of clean (111) surfaces; (0001) for Mg. All values are in electron volt.

	Au	Ag	Al	Mg	Ca
GGA	5.25	4.50	4.08	3.74	2.98
LDA	5.52	4.90	4.21	3.93	3.08
Expt.	5.26,[a] 5.35[b]	4.46,[c] 4.50,[d] 4.56[e]	4.24[f]	3.78[g]	(2.87)[h]
Calc.	5.27,[i] 5.35[b]	4.42[j]	4.25[k]	3.76,[l] 3.88[m]	2.86[n]

[a]Reference 86.
[b]Reference 17.
[c]Reference 87.
[d]Reference 88.
[e]Reference 89.
[f]Reference 90.
[g]Reference 91.
[h]polycrystalline value, Ref. 92.
[i]GGA, Ref. 93.
[j]GGA, Ref. 94.
[k]LDA, Ref. 95.
[l]LDA, Ref. 96.
[m]GGA, Ref. 96.
[n]LDA, Ref. 97.

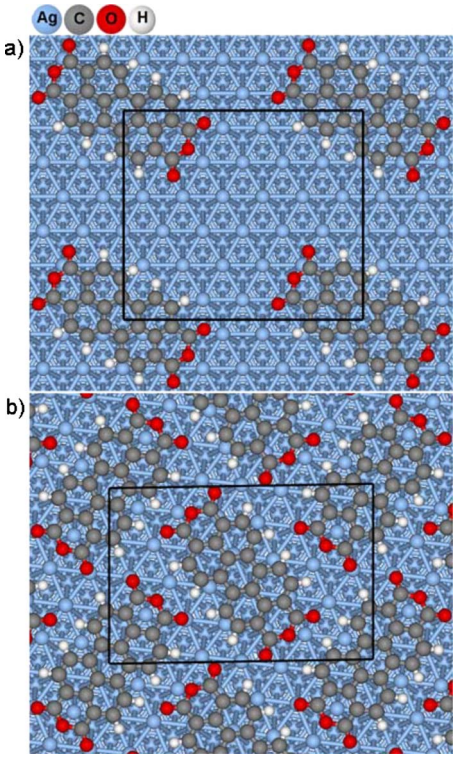

FIG. 1. (Color online) PTCDA monolayers on the Ag(111) surface. The solid lines denote the surface unit cells used in the calculations; (a) the dilute structure (with area $A=268$ Å^2); (b) the herringbone structure ($A=243$ Å^2).

A. Structure of adsorbed monolayers

PTCDA monolayers adsorbed on Ag(111) and Au(111) surfaces have been studied in detail experimentally.[48–55,98–100] In a close-packed monolayer the PTCDA molecules lie flat on the surface in a "herringbone" structure with the centers of the PTCDA molecules located on surface bridge sites.[49] The surface unit cell contains two PTCDA molecules, see Fig. 1(b). The experimental distances between the carbon rings of the molecules and the surface atoms are 2.86 Å and 3.27 Å for adsorption on Ag(111) and Au(111), respectively.[55,101] Experiments indicate a weak interaction between PTCDA and Au(111), consistent with physisorption,[50,100] and a somewhat stronger interaction between PTCDA and Ag(111).[49–53] PTCDA binds more strongly to open Ag surfaces and to surface steps.[102] We do not know of any such detailed studies on the structure of PTCDA adsorbed on the other metal (111) surfaces. We refrain from comparing our results to experiments where metals are deposited onto thin films of PTCDA, as this often leads to interdiffusion, which complicates the interpretation.[103–107]

In our calculations we use the herringbone structure of PTCDA on Ag shown in Fig. 1(b).[53] The unit cell has $\sqrt{43} \times \sqrt{19}$ periodicity with 33 metal atoms per layer in the Ag substrate. Since the lattice parameters of Au, Ag, and Al are similar, see Table I, we use a similar cell for PTCDA on these surfaces. For Mg and Ca, we choose a herringbone structure that results in a packing density of PTCDA molecules similar to that on the other surfaces. This results in 30 and 20 atoms per metal layer for Mg and Ca, respectively.

TABLE III. Average bond lengths (in Å) and bond angle of PTCDA adsorbed on Ag(111).

	LDA dilute	GGA dilute	GGA herringbone
C-H	1.10	1.09	1.09
C-C	1.42	1.43	1.43
C-O[a]	1.22	1.23	1.23
C-O[b]	1.38	1.40	1.40
C-O-C (deg)	125.2	125.3	124.7

[a]Carboxyl.
[b]Anhydride.

To study the effect of the packing density of PTCDA molecules, we also perform calculations on the structure used by Picozzi *et al.*,[108] see Fig. 1(a). This surface unit cell contains one PTCDA molecule. We refer to this structure as the "dilute" structure. The unit cell has $6\times3\sqrt{3}$ periodicity with 36 metal atoms per layer, so that the coverage of PTCDA molecules is $\sim\frac{1}{2}$ ML. The surface unit cells for the other metal substrates are chosen such that the coverage remains close to this value. The distance between the PTCDA molecules is then sufficiently large for the molecules to have no direct interaction. As it is easier to vary the geometry of the molecule and substrate in the dilute structure, as compared to the close-packed herringbone structure, we use the former to study the energetics of PTCDA adsorption. The optimized geometries of the PTCDA molecules in the two structures are very similar, as demonstrated by Table III, suggesting that close packing the molecules in the herringbone structure does not lead to a large intermolecular interaction. In addition, the GGA or LDA optimized geometries are very similar.

Common DFT functionals describe strong chemical interactions well, but they fail to capture weaker (van der Waals) bonding correctly. Using GGA functionals to describe the physisorption of closed-shell molecules on metal surfaces can lead to underestimating the binding energy and overestimating the bond distance between molecule and surface. This has also been found for the adsorption of an extended system as graphene on metal surfaces.[109,110] Using LDA functionals can lead to a serious overbinding and an equilibrium distance that is too small.[36,111] In the case of adsorbed graphene the LDA results on binding and equilibrium distance agree with experiment, however.[109,110]

Previous GGA calculations of the binding energy of PTCDA on Ag(111) give slightly varying results, i.e., a moderate binding of $\sim$0.5 eV/molecule,[102] or a very weak binding of $\lesssim$0.1 eV/molecule, or even a purely repulsive binding curve.[53,56,108,112,113] In the calculations where binding was obtained, the equilibrium distance ($\sim$3.4 Å) is significantly larger than the experimental equilibrium distance (2.9 Å).[51,55] Approximative schemes exist to incorporate van der Waals interactions in a DFT/GGA calculation.[114,115] For PTCDA on Ag(111) this increases the binding energy to $\sim$2 eV, but it does not significantly improve the GGA equilibrium distance.[56] For adsorption of graphene on metal sub-

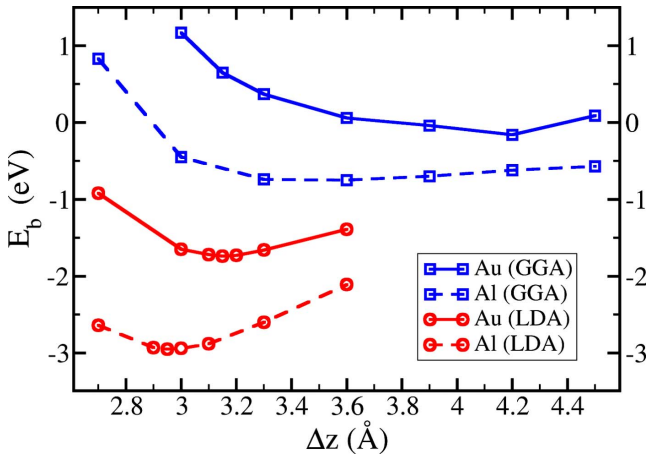

FIG. 2. (Color online) Binding-energy curves for (planar) PTCDA on Au(111) (squares) and Al(111) (circles). GGA and LDA values are indicated by the dashed and solid lines, respectively.

strates this scheme gives results that are inconsistent with experiment.[116] LDA calculations on PTCDA on Ag(111) give equilibrium distances of 2.8 Å (Ref. 108) and 2.7 Å,[53] which are in better agreement with experiment. The LDA binding energy, ~3 eV/molecule, however, is suspiciously large.[53] A calculation based on exact exchange and random-phase approximation correlation gives a binding energy and equilibrium distance that are quite close to the LDA values.[117]

We obtain very similar results in our GGA and LDA calculations for PTCDA on Ag(111). To illustrate how general this trend is, Fig. 2 shows binding-energy curves calculated with the dilute structure, where we varied the distance between the PTCDA layer and the Au and Al(111) surfaces. The GGA results for PTCDA on Au lead to an extremely shallow binding curve with a minimum at a distance >4 Å and a very small binding energy of ~0.1 eV/molecule. Using GGA for PTCDA on Al gives a sizable binding energy (~0.8 eV/molecule) and an equilibrium distance ~3.5 Å. LDA calculations lead to much larger binding energies, i.e., 1.7 eV/molecule for PTCDA on Au and 3.0 eV/molecule for PTCDA on Al. The corresponding equilibrium distances are 3.15 Å and 2.95 Å, respectively. An LDA calculation for PTCDA on Ag gives an equilibrium distance of 2.75 Å, which is somewhat smaller that the experimental value.

In conclusion, GGA and LDA give different results for the binding in weakly bonded systems. GGA gives small molecule-surface binding energies and large equilibrium distances, whereas LDA gives large binding energies and smaller equilibrium distances. As the reactivity of the surface increases along the series Au, Ag, Al, Mg, and Ca, one expects the adsorption of PTCDA gradually changing from physisorption to chemisorption. The differences between the GGA and LDA become smaller and the results more reliable. For PTCDA on Mg(0001) and Ca(111) we obtain GGA binding energies of 2.3 eV/molecule and 8.4 eV/molecule, respectively, indicative of chemical bonding.

We also find that, if the binding energy increases, the PTCDA molecule looses its planar geometry. If the interaction between the PTCDA molecule and the surface is large,

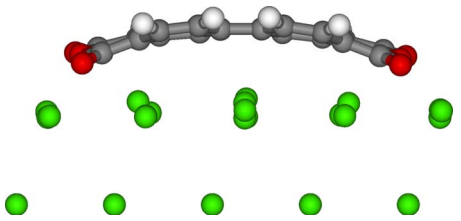

FIG. 3. (Color online) Optimized geometry of the arching PTCDA molecule on the Ca(111) surface.

the molecule arches as shown in Fig. 3. The effect is similar to what is found for other molecules, such as tetrafluorotetracyanoquinodimethane (F4TCNQ).[118,119] The extend of this geometry deformation depends on the metal substrate. Optimizing the geometry of PTCDA on Ca with GGA and defining the position of the surface by the average z coordinate of the top layer of Ca atoms, we find that the outer carbon atoms of the perylene core are 0.8 Å closer to the surface than the carbon atoms in the center. The latter have a distance of 2.6 Å to the surface. Such short distances are indicative of a strong interaction between molecule and surface. A geometry deformation also occurs in the end groups of the PTCDA molecule, where the carboxyl oxygen atoms move toward the surface, and the anhydride oxygen moves away from the surface. A strong deformation of the PTCDA molecule is accompanied by a rumpling of the surface, where metal atoms are lifted out of the surface, decreasing the distance with the molecule. For instance, the distances between the carboxyl oxygen atoms and the nearest Ca atoms are 2.3 Å. Such short distances suggest the formation of bonds, which matches the large binding energy of 8.4 eV/molecule.

The deformation of the adsorbed PTCDA molecule and that of the metal substrate decrease through the series Ca, Mg, Al, Ag, and Au, and is accompanied by a decrease in the binding energy. The deformation pattern of the PTCDA molecule qualitatively remains the same along this series, but the amplitude of the deformation decreases. For instance, the (GGA) distances between the carboxyl oxygen atoms and the nearest Mg atoms are 2.4 Å and the outer carbon and core carbon atoms are at 2.6 Å and 2.8 Å from the surface, respectively. This matches the binding energy of 2.3 eV/molecule, which is much less than between PTCDA and Ca(111). Throughout the series Al, Ag, and Au the binding energy, as well as the geometric deformation of the molecule, decrease monotonically.

For instance, if we fix the overall PTCDA-Ag(111) distance at 2.75 Å and optimize the geometry, the molecule is only slightly arched. The outer carbon atoms are 0.1 Å closer to the surface than the core carbon atoms. The carboxyl oxygen atoms are 0.2 Å closer to the surface, whereas the anhydride oxygen atoms are at approximately the same height as the core carbon atoms. This pattern is in fair agreement with experimental observations.[51] At the end of the series, i.e., for PTCDA on Au(111), the binding energy is vanishingly small and the molecule and surface have an undistorted, planar geometry. The binding energies and geometries of PTCDA on Al and Ag obtained in previous calculations follow the trends discussed above.[56,108,112,113]

B. Work functions

From the calculations discussed in the previous section we can understand the trends in the bonding and in the geometry of PTCDA adsorbed on the different metal surfaces. In this section we study the work function changes induced by the adsorption, which originate from a redistribution of charge at the MOI. The charge distribution is mainly determined by electrostatic and short-range exchange correlation interactions, which are represented well by LDA and GGA functionals.[114,115] For example, the charge transfer between the weakly interacting molecules in a charge-transfer crystal is described well by LDA,[120] as is the work-function graphene adsorbed on a metal surface.[109,110] Given the bonding geometry of the molecule and surface, we expect therefore these functionals to give good values for the work function of molecular monolayers adsorbed on a metal surface. However, since they do not incorporate van der Waals interactions correctly, calculations lead to a considerable uncertainty in the molecule-surface equilibrium distance for weakly bonded systems, as discussed in the previous section. Because of this uncertainty we investigate the formation of interface dipoles in a number of steps. We start with the dilute structure and perform calculations for fixed molecule surface distances d in the range 3.0–3.6 Å. Results obtained with GGA and LDA are then compared. In the second step we switch to the more densely packed herringbone structure that is observed experimentally, which allows us to study the effect of the packing density. Finally, we discuss the effects of full geometry relaxation of the molecules and the surface.

Figure 4(a) shows the work functions for a layer of planar PTCDA molecules adsorbed in the dilute structure on the different metal surfaces, calculated using the GGA functional. One immediate observation is that adsorption on Au(111) leads to a lowering of the work function as compared to the clean surface, whereas adsorption on the other metal surfaces leads to an increase in the work function. There is some dependence of the work function on the distance between the molecule and the surface, but it is not excessively large. By fitting a straight line through the curves in Fig. 4(a) one obtains [see Eq. (1)] $S=0.5$ at $d=3.6$ Å and $S=0.6$ at $d=3.0$ Å. These values are considerably lower than the $S=1$ that follows from the Schottky-Mott rule, indicating that significant interface dipoles are formed upon adsorption. Since the work-function changes decrease somewhat upon decreasing the molecule-surface distance, the interface dipoles decrease with decreasing distance. The calculated values for S are much higher than the $S\approx 0$ obtained experimentally.[8,22] We will show below that this discrepancy is resolved by increasing the packing density of the PTCDA molecules, which is only $\sim\frac{1}{2}$ ML in the dilute structure.

To illustrate the effect of using a different functional, Fig. 4(b) gives the work functions for the dilute structure at fixed distances between the molecule and the substrates, calculated using the LDA functional. Compared to the GGA results of Fig. 4(a), the LDA work functions are generally somewhat higher, as was also the case for the clean metal surfaces, see Table II. The changes in the work functions upon adsorption calculated with LDA or GGA, are comparable, however, at the same molecule-surface distance. It means that, although

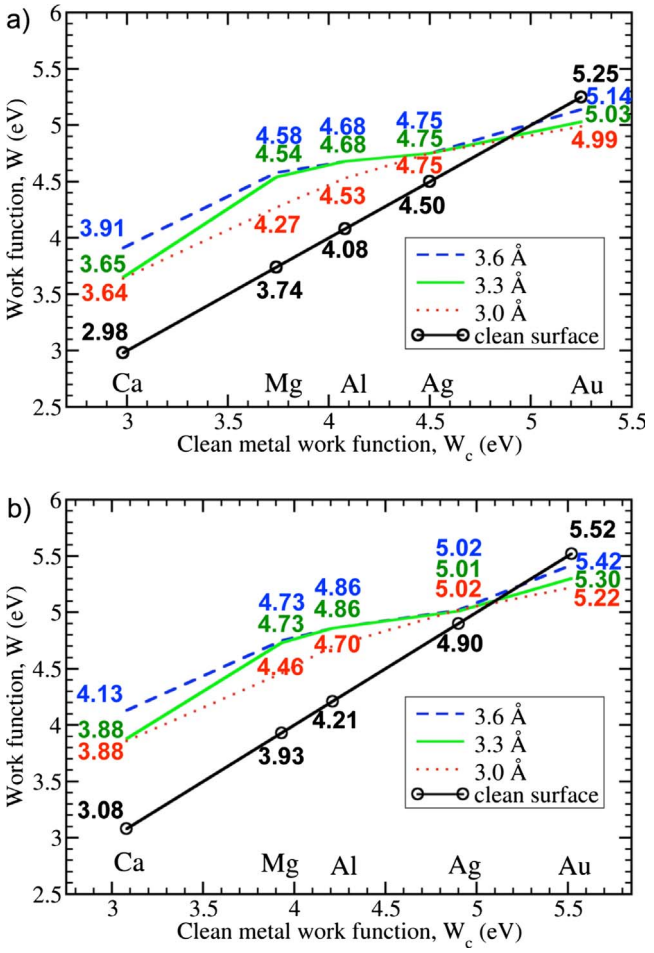

FIG. 4. (Color online) Work functions of a PTCDA monolayer on (111) metal surfaces [(0001) for Mg] in the dilute structure, calculated using (a) the GGA and (b) the LDA functionals. The clean metal work function is given along the x axis. The numbers give the calculated values, the lines guide the eyes. The bottom (black) curve refers to the clean metal surfaces. The top three curves are for different distances d between the PTCDA molecules and the surfaces.

the binding between the molecules and the surfaces calculated with LDA or GGA can be considerably different, as discussed in the previous section, the charge redistribution upon adsorption is similar, if we consider the same molecule-surface distance. Since the GGA work functions of the clean metal surfaces are somewhat closer to the experimental values, see Table II, we will use GGA values for the adsorbed layers in the following.

Figure 5 shows the work functions of the herringbone structure of PTCDA on metal surfaces, calculated using the GGA functional. As for the dilute structure, Fig. 4(a), adsorption on Au(111) lowers the work function, and on the other metal surfaces it increases the work function. In the herringbone structure the work-function shifts are much larger, however. Most strikingly, as one can observe in Fig. 5, the work function is pinned at ~4.7 eV over a considerable range of metal substrates and molecule-surface distances. The pinning leads to $S=0$. Deviations from pinning are observed only for low work-function metals and short molecule-surface dis-

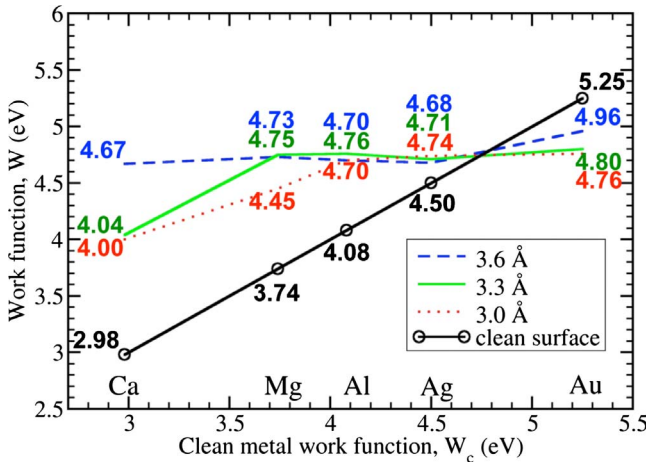

FIG. 5. (Color online) As Fig. 4 for PTCDA in the herringbone structure.

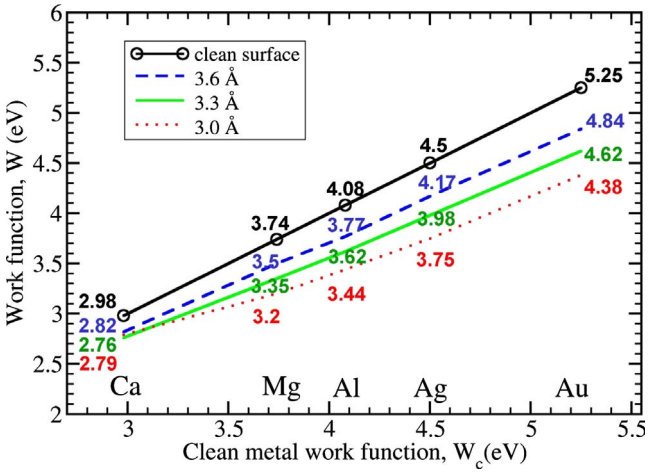

FIG. 6. (Color online) As Fig. 4 for benzene in a $(\sqrt{7}\times\sqrt{7})R19.1°$ structure (Ref. 62).

tances, i.e., $d \leq 3.3$ Å for Ca and $d=3.0$ Å for Mg.

Experimentally reported values for work functions of PTCDA adsorbed on Au(111) are 4.8,[8,22] 4.75,[57] and 4.79 eV.[58] For PTCDA adsorbed on Ag(111) reported values are 4.9,[52] 4.75,[57] and 4.51 eV.[58] For PTCDA adsorbed on a range of metal substrates with clean metal work functions ranging from 3.8 eV (Mg) to 5.2 eV(Au) pinning of the work function has been observed at a value close to 4.8 eV.[8,22] The fact that there is pinning, as well as the value of the pinned work function, are in agreement with our findings.

LDA gives very short molecule-surface distances, which can serve as lower bounds $d_{\min}$. We have optimized the geometries at $d_{\min}$ of an adsorbed PTCDA monolayer in the herringbone structure and calculated the work functions with GGA, see Table IV. These work-function results for adsorption on Au, Ag, and Al(111) are very close to the pinning value in Fig. 5. The work functions for adsorption on Mg(0001) and Ca(111) drop to a lower value. As discussed in the previous section, the Ca and Mg surfaces become somewhat unstable at $d_{\min}$, i.e., metal atoms are pulled up from the surface, which is accompanied by a strong arching distortion of the PTCDA molecule. Such a deformation generates a molecular dipole moment perpendicular to the surface that decreases the work function.[56]

IV. BENZENE AND PERYLENE

Although there is some spread in the numbers measured, experiments clearly indicate a lowering of the work function after adsorption of a benzene monolayer on several metal surfaces. Measured work-function shifts are 0.18 eV on Al(111),[62] 0.3 and 0.7 eV on Ag(111),[59,60,63] 0.7 and 1.05 eV on Cu(111),[37,61] and 1.10 eV on Au(111).[37] Previous GGA calculations for benzene on Al(111) gave an equilibrium distance of 3.7–3.8 Å.[62] Quantum chemical MP2 calculations for a single benzene molecule adsorbed on a cluster of metal atoms gave equilibrium distances of 3.8 Å for benzene on Au(111) and 4.0 Å for benzene on Cu(111).[37] We calculate the work functions of a benzene monolayer adsorbed on different metal surfaces at a set of fixed distances in the same way as discussed in the previous section. A $(\sqrt{7}\times\sqrt{7})R19.1°$ structure is used as in Ref. 62, which gives a somewhat less than close-packed coverage of the surfaces.

TABLE IV. LDA optimized molecule-surface distances $d_{\min}$ and GGA work functions W of PTCDA monolayers in the herringbone structure, adsorbed on metal(111) [for Mg(0001)] surfaces.

	$d_{\min}$ (Å)	W (eV)
Au	3.15	4.78
Ag	2.75	4.65
Al	2.95	4.68
Mg	2.7–2.8	3.80
Ca	2.3–2.4	3.39

The (GGA) results are given in Fig. 6. The most important observation is that adsorption of benzene leads to a decrease in the work function for all the surfaces studied. This is very different from the effect of PTCDA adsorption, see Figs. 4 and 5. Moreover, adsorption of benzene gives a work-function lowering that is of a similar size for all surfaces (at a fixed molecule-surface distance). This leads to $S=0.9$ at $d=3.6$ Å and $S=0.8$ at $d=3.0$ Å, which is not extremely far from the Schottky-Mott limit $S=1$. The absolute size of the work-function shift depends on the molecule-surface distance with the number at $d=3.0$ Å being roughly twice as large as that at $d=3.6$ Å. The sign of the work-function shift, its relatively weak dependence on the metal, and its sensitivity to the molecule-metal distance all point to an interpretation in terms of the pillow effect. The effect is determined by the Pauli repulsion between the molecular and surface electrons, which decreases the surface dipole and therefore the work function.[33,34,37] Pauli repulsion critically depends on the overlap between the molecular and surface wave functions and therefore on the distance between the molecule and the surface. Our calculations and previous calculations[37,62] suggest that the distances between the benzene molecule and the metal surfaces are rather large, i.e., $\gtrsim 3.5$ Å.

Summarizing, adsorption of the large PTCDA molecule leads to work-function pinning ($S \approx 0$), and adsorption of the small benzene molecule gives a uniform work-function

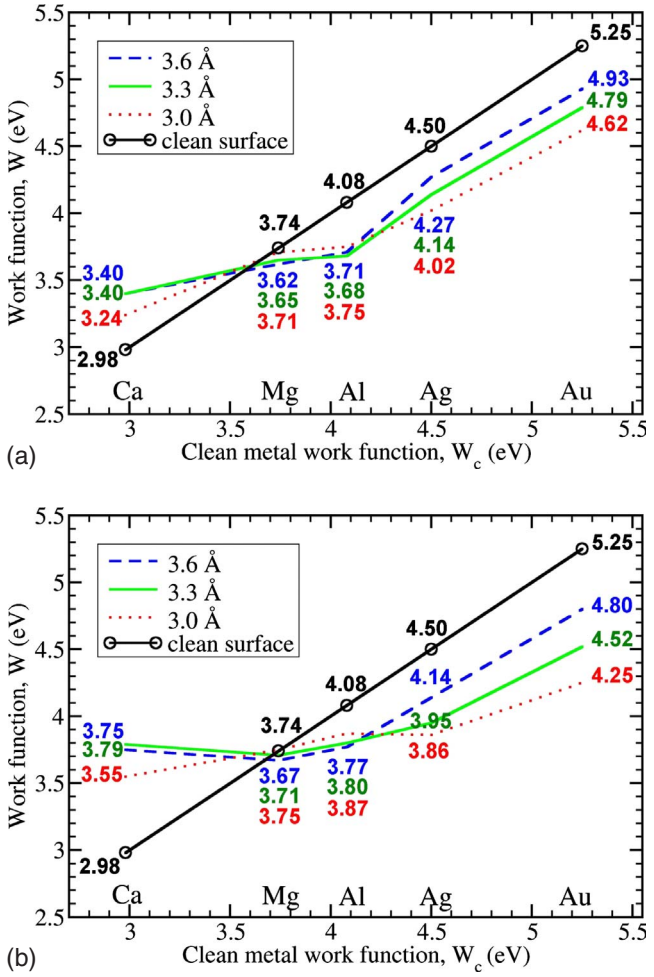

FIG. 7. (Color online) As Fig. 4 for perylene in (top) the dilute structure and (bottom) the herringbone structure.

lowering ($S \approx 1$). It is then interesting to study the adsorption of an intermediately sized molecule, such as perylene. The structure of a perylene monolayer on a metal surface is less well established than that of a PTCDA monolayer. A herringbone structure similar to PTCDA is the structure proposed for a close-packed perylene monolayer on Ag(111) and Au(111).[50,64,65] Ultraviolet photoemission spectroscopy (UPS) measurements give a decrease in the work function of perylene on Au and Ag by 0.8 eV and 0.6 eV, respectively, and an increase in the work function of perylene on Ca by 0.3 eV.[66]

We perform calculations for a perylene monolayer adsorbed on different metal surfaces at a set of fixed distances. Analogous to PTCDA we use two different structures, i.e., a close-packed herringbone structure, and a dilute structure. The unit cell of the herringbone structure of perylene on Ag(111) has $5 \times 2\sqrt{3}$ periodicity containing 20 metal atoms per layer.[65] That of the dilute structure has $5 \times 3\sqrt{3}$ periodicity, so the packing density of the perylene molecules is 1/3 ML. The unit cells on Au and Al are the same, and those on Mg and Ca are chosen such that they lead to similar structures and packing densities. The calculated work functions are shown in Fig. 7. Two regimes can be distinguished. For the high work-function surfaces (Au, Ag), adsorption of perylene leads to a lowering of the work function, whereas for the low work-function surface of Ca, adsorption of perylene increases the work function. These results are in qualitative agreement with experiment. The curves in Fig. 7 indicate that the transition between these two regimes takes place in the range Mg-Al.

From these curves the transition between the two regimes can be quantified. Starting with the results obtained for the dilute structure at a molecule-surface distance $d=3.6$ Å, a line through the points for Ca, Mg, and Al gives $S=0.3$ whereas a line through the points for Al, Ag, and Au leads to $S=1.0$. For the herringbone structure the same procedure for $d=3.6$ Å gives $S=0$ and 0.9, respectively. It is instructive to compare these S values to the values obtained for benzene and PTCDA. It suggests that for Ca, Mg, and Al one obtains pinning of the work function upon perylene absorption, similar to PTCDA, see Fig. 5, whereas for Ag and Au one finds a uniform work function decrease, similar to benzene, see Fig. 6. Upon decreasing the distance between the perylene molecules and the surfaces the S values in the high- and low-work-function regimes become somewhat closer and the transition between the two regimes becomes less sharp. Note that the distance dependence in the low-work-function regime resembles the distance dependence of the PTCDA case, whereas in the high-work-function regime it resembles the benzene case. Experimentally such a transition is observed for Alq_3 adsorbed on different surfaces. For adsorption on low-work-function metals $S \approx 0$, whereas for adsorption on high-work-function metals $S \approx 1$.[39]

V. DISCUSSION

The results presented in Fig. 5 show that adsorption of a PTCDA monolayer pins the work functions at ~4.7 eV for a broad range of distances. The fact that one gets pinning, as well as the value of the pinning level, are in good agreement with experimental observations. The results obtained for benzene and perylene adsorption are in qualitative agreement with available experimental results, i.e., adsorption of benzene leads to a lowering of the work function in all cases, and adsorption of perylene gives a work function decrease for high-work-function metals and a work function increase for low-work-function metals. In this section we analyze this behavior and interpret the results. First we analyze the density of states, then we consider explicitly the charge transfer at the molecule-substrate interface, and finally we formulate a simple phenomenological model.

A. Density of states

Figure 8 (top) gives the KS DOS of an isolated PTCDA molecule, calculated using the GGA functional. The energies of the highest occupied molecular orbital (HOMO) and the lowest unoccupied molecular orbital (LUMO) are at −6.24 eV, respectively, −4.64 eV with respect to the vacuum level. The KS spectrum is similar to that obtained in previous DFT calculations.[30,104,121,122] The GGA HOMO-LUMO gap of 1.60 eV also agrees with the value found in other GGA calculations.[30,108]

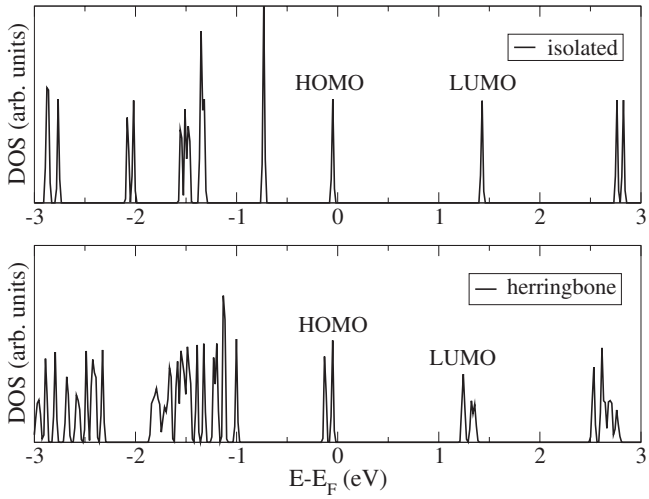

FIG. 8. Top: total DOS of an isolated PTCDA molecule calculated using a Gaussian broadening of 0.01 eV. The HOMO and the LUMO are indicated. The energy is set to zero at the position of the HOMO. Bottom: total DOS of a free-standing PTCDA monolayer in the herringbone structure, see Fig. 1.

The interpretation of KS energy levels is the subject of a long-standing debate. From calculations with advanced functionals it is argued that the KS energies of all occupied molecular orbitals should correspond to vertical ionization potentials (IPs), as can be extracted from a photoemission spectrum, for instance. Approximative functionals such as GGA then still give a reasonable ionization spectrum, but it is shifted to a higher energy by approximately a constant.[123,124] The work function is the lowest IP of an extended system. Even approximative functionals such as GGA or LDA usually give work functions that are close to the experimental values, as is illustrated by Table II. Results of a similar quality are obtained for work functions of adsorbed atomic and molecular layers.[16–21]

The KS energy levels corresponding to unoccupied molecular orbitals generally do not have such a simple interpretation. In particular, the energy of the DFT LUMO (ϵ_0) should not correspond to the EA even with the exact DFT functional. From calculations with accurate functionals it is shown that $\epsilon_0 < -\mathrm{EA}$, both for molecules,[125] as well as for extended systems.[126,127] The difference between $|\epsilon_0|$ and the EA can be several electron volt, which is attributed to the fact that an accurate functional has a discontinuous derivative as function of the number of electrons.[126,127]

A similar difference is found for approximative continuous functionals such as GGA or LDA. However, it is well known that for these approximative functionals, Slater's transition state approach allows for a simple estimate of the EA.[128] We define ϵ_0 as the KS energy of the LUMO of the neutral molecule, and $\epsilon_M(1)$ as the KS energy of the singly occupied HOMO of the ion that has one additional electron. The functionals allow for a fractional occupancy of the level ϵ_M with N electrons, and using Janak's theorem[129]

$$\epsilon_M = \frac{\partial E_{\mathrm{tot}}}{\partial N}, \tag{4}$$

where E_{tot} is the total energy, one can write

$$\mathrm{EA} = -\int_0^1 \epsilon_M(N)dN. \tag{5}$$

To a good approximation the dependence of ϵ_M on the occupancy is linear and can be parameterized as

$$\epsilon_M(N) = \epsilon_0 + UN, \tag{6}$$

where U is the effective charging energy per electron.[130,131] This then gives

$$\mathrm{EA} = -\epsilon_0 - \frac{1}{2}U. \tag{7}$$

This procedure gives results that agree very well with charging energies for isolated conjugated molecules extracted from total-energy calculations.[10] In the following we use the terms HOMO and LUMO in the KS context, and refer to IP and EA for the measurable properties of the molecule.

From separate self-consistent-field (SCF) calculations on the neutral molecule and the singly charged ion one can extract ϵ_0 and $\epsilon_M(1)$, and calculate $U=\epsilon_M(1)-\epsilon_0$. Following this procedure, we extract a charging energy $U=3.31$ eV from calculations on PTCDA^0 and PTCDA^-. Using the LUMO energy $\epsilon_0=-4.64$ eV, we then find from Eq. (7) EA=2.98 eV for PTCDA. This value is in very good agreement with the value EA=2.96 eV we extract from a ΔSCF total-energy difference calculation. Slater's transition state approach can also be used to calculate the IP. Assuming that the charging energy for holes on PTCDA is the same as for electrons and using the HOMO energy of −6.24 eV, then yields IP=7.90 eV, which is in fair agreement with the experimental PTCDA gas phase IP of 8.15 eV cited in Ref. 121.

If a molecule is embedded in a crystal, its charging energy U is reduced drastically because of screening by the surrounding crystal.[10,132] One can write

$$U = U_{\mathrm{bare}} - 2P^-, \tag{8}$$

where U_{bare} is the charging energy of a bare molecule and P^- is the polarization energy associated with a singly charged molecular ion in a crystal.[133] Using the polarization energy $P^-=0.91$ eV from Ref. 132, we obtain an effective charging energy of a PTCDA molecule embedded in a PTCDA crystal $U_{\mathrm{cryst}}=3.31-1.82=1.49$ eV. Slater's transition state model then gives $\mathrm{EA}_{\mathrm{cryst}}=3.90$ eV and $\mathrm{IP}_{\mathrm{cryst}}=6.99$ eV for the EA and IP of a PTCDA molecule in the crystal. This leads to a transport gap $E_t=\mathrm{IP}_{\mathrm{cryst}}-\mathrm{EA}_{\mathrm{cryst}}=3.09$ eV. The values of the IP and E_t are in good agreement with the values extracted from experiment, i.e., 6.7 ± 0.2 eV and 3.2 ± 0.4 eV, respectively.[57,134]

In summary, using the KS DOS as shown in Fig. 8, to calculate measurable quantities, one has to incorporate the charging energy U of the molecule, cf. Eqs. (6) and (7). U strongly depends on the interaction of the molecule with its environment. Screening by a metal substrate reduces U significantly, for instance.[132,134]

Before considering the DOS of adsorbed PTCDA layers, we look at the DOS of a free-standing PTCDA monolayer in the herringbone structure, shown in Fig. 8 (bottom).

The interaction between PTCDA molecules in the monolayer is not negligible (with an interaction energy ~0.6 eV/molecule),[56,122] which changes the DOS compared to that of the isolated PTCDA molecule, Fig. 8 (top). Some peaks are doubled, such as the ones corresponding to the HOMO and LUMO, because the two molecules in the unit cell of the herringbone structure are not exactly equivalent.[53] The HOMO-LUMO gap decreases somewhat, going from ~1.6 eV in the isolated molecule to ~1.4 eV in the monolayer. The most prominent changes affect the peaks originating from oxygen lone-pair dominated states of the PTCDA molecule, such as the HOMO-1 state in Fig. 8 (top). The orbitals corresponding to these lone-pair states lie foremost in the plane of the molecule. Their involvement in the intermolecular (hydrogen) bonding in the PTCDA layer shifts the corresponding peaks to lower energy, cf. Fig. 8 (bottom).

We now consider the DOS of PTCDA monolayers adsorbed on metal surfaces. Since the full DOS is dominated by states originating from the metal substrate, we look at the DOS projected on the carbon atoms of the molecule [projected DOS (PDOS)], in order to identify the contributions of the molecular levels. Figure 9 gives the PDOSs of PTCDA monolayers adsorbed on metal surfaces at distances of d =3.0 and 3.6 Å. We have applied a Gaussian broadening with a broadening parameter of 0.1 eV to avoid a spiky appearance of the PDOS. Comparison to Fig. 8 allows us to identify the contributions of the molecular levels, in particular those states that are dominated by the molecular HOMO and LUMO. Although all states result from hybridization between molecular and metal states, it simplifies the analysis if we label them by their dominant molecular character.

The interaction between the molecule and the surfaces induces hybridization of molecular and metal states. For adsorption on simple, wide-band metals this leads to a simple broadening of the molecular levels into resonances.[135] For adsorbed PTCDA, the extend of this broadening is moderate. At d=3.6 Å the typical width at half height of the HOMO and LUMO peaks is ~0.2 eV. The widths increase with decreasing molecule-metal distances (to ~0.3 eV at d =3.0 Å, for instance). These results agree with the widths found in previous DFT calculations of adsorbed PTCDA,[108] as well as with those typically found for other adsorbed molecules such as pentacene.[111] They are also in qualitative agreement with peak widths observed in scanning tunneling spectroscopy of PTCDA adsorbed on Ag and Au(111) surfaces.[53,54,100] The widths found in the calculations of Refs. 30 and 31 are much larger.

Comparing the two columns in Fig. 9, one observes that the PDOSs at the two distances are qualitatively similar, but that the spectrum at d=3.0 Å is shifted toward lower energy as compared to the spectrum at d=3.6 Å by up to 0.5 eV, depending on the metal substrate. This is caused by the pillow effect, as we will discuss in Sec. V C. The HOMO-LUMO gap of PTCDA decreases somewhat with the adsorption strength, from ~1.4 eV (peak maximum to peak maximum) for PTCDA weakly interacting with Au(111), which is comparable to the gap of the PTCDA free-standing monolayer, Fig. 8(b), to ~1.1 eV for PTCDA strongly interacting with Ca(111).

One observation that can be made by comparing Figs. 5 and 9 is that work-function pinning occurs when the Fermi level crosses the level of the LUMO. For PTCDA on Au the LUMO is unoccupied, but already for PTCDA on Ag the LUMO gets partially occupied. This implies that electron transfer takes place from the metal substrate to the molecule. Judging from the upwards shift of the Fermi level along the columns of Fig. 9 the amount of electron transfer increases along the series Ag, Al, Mg, and Ca. As long as the Fermi level is inside the LUMO peak, the work function is pinned, compare Fig. 5. At the short molecule-surface distance of 3.0 Å between PTCDA and Ca, the Fermi level jumps to the next peak, i.e., the LUMO+1, see Fig. 9(i). This is accompanied by an "unpinning" of the work function, compare Fig. 5.

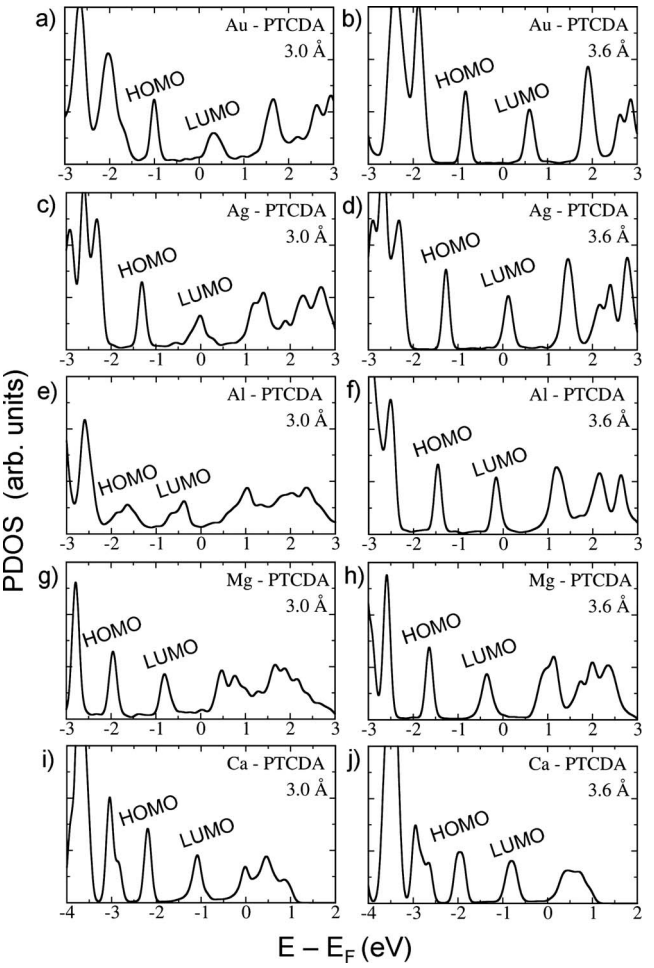

FIG. 9. PDOS of the PTCDA molecule adsorbed on metal surfaces at a fixed distance d in the herringbone structure, calculated using a Gaussian broadening of 0.1 eV; left: d=3.0 Å; right: d =3.6 Å. The peaks corresponding to the molecular HOMO and LUMO levels are labeled.

The most detailed experiments have been performed for PTCDA on Ag(111). In UPS and scanning tunnel microscopy (STM) experiments a peak is observed at the Fermi level that is identified as the LUMO of the PTCDA molecule, whereas a peak at ~−1.6 eV with respect to the Fermi level is labeled as the HOMO.[52–54,57] In Fig. 9(c), where the distance between PTCDA and the Ag surface is close to the experimental value, we find the HOMO at −1.3 eV and the LUMO

at the Fermi level, which is in reasonable agreement with the experimental analysis. In STM and inverse photoelectron spectroscopy (IPES) experiments of PTCDA on Au(111) a peak is observed at 1.0–1.5 eV above the Fermi level that is associated with the EA level of the molecule.[100,132,136] Applying Eqs. (7) and (8) puts the EA level at P^- above the LUMO in Figs. 9(a) and 9(b). Using the polarization energy $P^-=0.97$ eV for a PTCDA ion adsorbed on a metal surface calculated in Ref. 132 then brings the EA level in the experimentally observed range.

Pinning of the work function at MOIs has been interpreted in terms of a charge neutrality level (CNL),[30–32] in analogy to Schottky barrier models for conventional semiconductors.[29,137,138] The CNL model relies on having a large continuum DOS at the metal-semiconductor interface, which fills the energy gap of the semiconductor. The Fermi level is then pinned by these metal-induced gap states (MIGS).[27] Conventional semiconductors such as Si or GaAs have reactive surfaces with surface atoms carrying dangling bonds. The energies of these dangling-bond states are within the semiconductor gap. Bonding at a metal-semiconductor interface leads to broadening of these states, which generates a large continuum DOS at the interface in the semiconductor gap.[139,140] Closed-shell molecules such as PTCDA do not have dangling-bond states within the HOMO-LUMO gap. The creation of a large DOS at a MOI within the HOMO-LUMO gap then depends on a large broadening of the molecular levels. We do not observe such a large broadening.

The DOS of an isolated perylene molecule resembles that of PTCDA. The GGA HOMO-LUMO gap of 1.8 eV is slightly larger than that of PTCDA. Figure 10 gives the PDOS on a perylene molecule adsorbed on metal surfaces at distances of $d=3.0$ and 3.6 Å. Comparison to Fig. 7(b) shows that pinning of the work function sets in as the Fermi level reaches the LUMO. In other words, as for PTCDA, the work function is pinned by the LUMO of the molecule. As the perylene LUMO lies ~1 eV higher than that of PTCDA, compare Figs. 9 and 10, the pinning level for adsorbed perylene is ~3.7 eV. For benzene we observe no pinning, see Fig. 6, as the LUMO level is too high in energy and is not populated even if benzene is adsorbed on a low-work-function metal-like Ca.

B. Charge transfer and interface dipole

The charge transfer at the PTCDA-metal interface can be visualized directly by calculating the laterally averaged electron-density difference

$$\Delta\bar{n}(z) = \bar{n}_{\mathrm{PTCDA/metal}}(z) - \bar{n}_{\mathrm{metal}}(z) - \bar{n}_{\mathrm{PTCDA}}(z). \qquad (9)$$

The electron density $\bar{n}_{\mathrm{metal}}$ and $\bar{n}_{\mathrm{PTCDA}}$ of the metal substrate and the molecule are obtained in separate calculations with the substrate and the molecule frozen in the adsorption geometry, using the same unit cell. The lateral averaging is done as in Eq. (3). Examples of $\Delta\bar{n}(z)$ are shown in Fig. 11.

Figures 11(a)–11(c) clearly show the formation of interface dipoles that are localized at the PTCDA/metal interface. Note that the sign of the interface dipole moment of PTCDA on Au is opposite to that of PTCDA on the other metal surfaces. For PTCDA on Au electrons are displaced from the molecular region into the metal, whereas for PTCDA on other metals electrons are displaced from the metal to the molecule. According to the PDOSs shown in Figs. 9(c)–9(j)

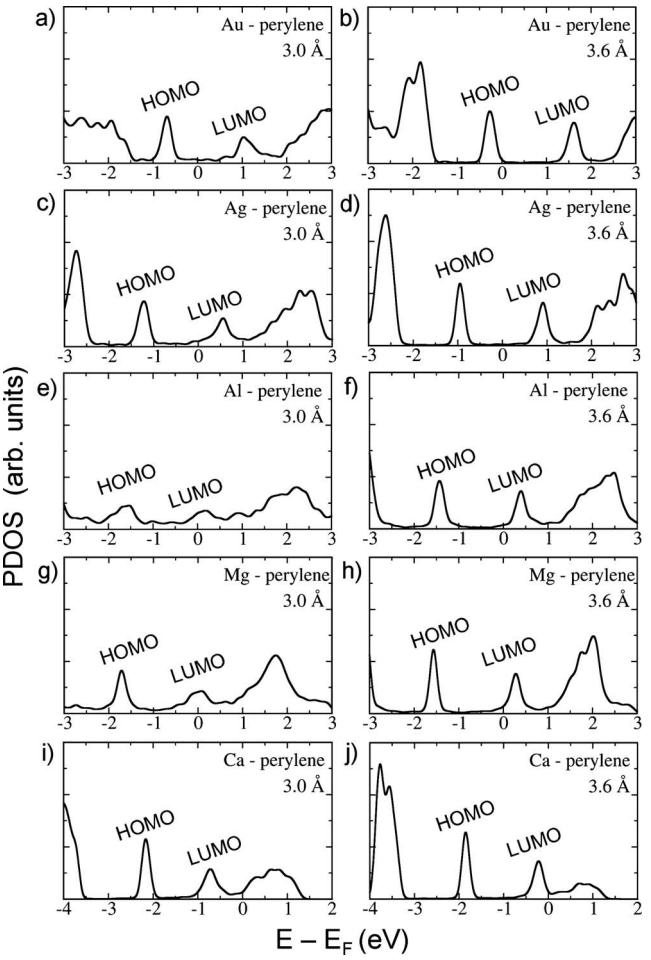

FIG. 10. As Fig. 9 for perylene adsorbed on metal surfaces.

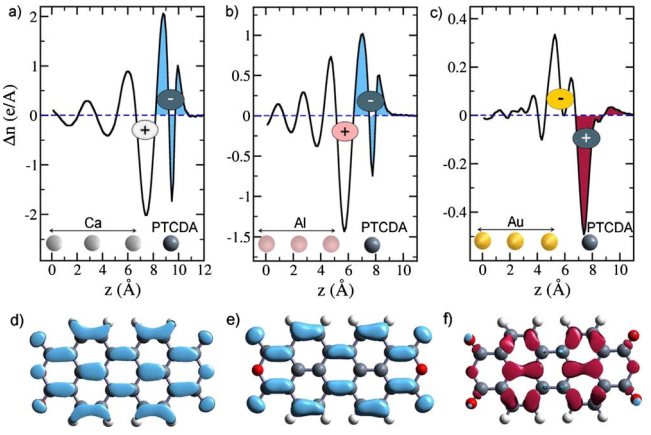

FIG. 11. (Color online) Laterally averaged electron-density difference $\Delta\bar{n}(z)$ for PTCDA adsorbed on (a) Ca(111), (b) Al(111), and (c) Au(111) at a fixed distance $d=3.0$ Å. The +/− indicate the direction of the interface dipole. The charge on the molecule is estimated by integrating over the shaded areas (see text). (d)–(f) Isodensity surface of $\Delta n(x,y,z)$ close to the molecular plane.

the latter can be interpreted as electron transfer from the metal to the LUMO of the molecule. In contrast, the displacement of electrons for PTCDA on Au cannot straightforwardly be related to the transfer of electrons to or from a molecular level, as can be observed from the PDOSs of Figs. 9(a) and 9(b).

The charge displacement for PTCDA on Au can be interpreted in terms of the pillow effect.[34,37] In case of a weak interaction between the molecule and the surface, the wave function of the system can be written in good approximation as an antisymmetrized product of the wave functions of the separate molecule and the substrate. This introduces the effects of exchange between the molecular and substrate electrons, leading to a repulsive interaction in case of a closed-shell molecule, called the Pauli repulsion. The electronic cloud of the molecule is usually less easily deformed than that of the metallic substrate. Therefore, the net effect of Pauli repulsion is that the molecular electronic cloud pushes back the substrate electronic cloud into the metal (as if the molecule lands on a pillow). The push back of electrons into the metal can be observed in Fig. 11(c). It lowers the surface dipole, and therefore it lowers the work function.

All molecular orbitals contribute to the pillow effect, but not to the same degree, as their contribution depends on the overlap integrals with the metal surface orbitals at the surface. Nevertheless, one may expect that the spatial distribution of the displaced electrons reflects the general shape of the molecule.[34,37] The pattern of electron depletion in the molecular region can be visualized by plotting $\Delta n(x,y,z)$, as is shown in Fig. 11(f). The pattern does not correspond to the HOMO of PTCDA,[122] showing that the electron depletion is not simply a transfer of electrons from the HOMO to the Au surface. This conclusion is consistent with the PDOSs of Figs. 9(a) and 9(b).

The change in electron density for PTCDA on other metals is qualitatively different from that of PTCDA on Au. Electrons are transferred from the metal to states of the molecule, which is clearly demonstrated by plotting $\Delta n(x,y,z)$. The nodal pattern of $\Delta n(x,y,z)$ for PTCDA on Al, Fig. 11(e), corresponds to the LUMO of PTCDA, indicating that electrons are transferred to this state, in agreement with Fig. 9(d). For PTCDA on Ca, Fig. 11(e), the nodal pattern shows both features of the LUMO and of the LUMO+1.[104] This agrees with Fig. 9(i), which shows that electrons are transferred to both these states.

One may calculate the interface dipole per adsorbed molecule as $\Delta\mu = eA\int z\Delta\bar{n}(z)dz$, with A the surface area of the adsorbed molecule. A more direct way to extract the interface dipole is from the change in the work function ΔW upon adsorption of the molecules, using the Helmholtz relation[141]

$$\Delta\mu = \frac{\varepsilon_0 A}{e}\Delta W. \tag{10}$$

The results are given in Table V. The total charge q on the molecule can be estimated by

TABLE V. Interface dipole per molecule $\Delta\mu$ [Eq. (10)] and total molecular charge q [Eq. (11)] for PTCDA on metal surfaces. The distance between the molecules and the surface is fixed at 3.0 Å.

Metal	$\Delta\mu$ (D)	$q(e)$
Au	−1.58	+0.34
Ag	0.77	−0.31
Al	2.00	−0.82
Mg	2.29	−0.84
Ca	3.29	−1.34

$$q = -e\int_{z_0}\Delta\bar{n}(z)dz, \tag{11}$$

where z_0 is the point between the molecule and the surface where $\Delta\bar{n}(z_0)=0$. The integration is indicated by shaded areas in Figs. 11(a)–11(c).[142]

Comparing the values for Ag to Ca in Table V, one notices an increase in the interface dipole and in the number of electrons transferred from the metal surface to the molecule. This is consistent with the change in the work function upon adsorption and with the PDOSs, see Figs. 5 and 8. The charge distributions of the interface dipole on Ag, Al, Mg, and Ca are similar. The distributions shown in Figs. 11(a) and 11(b) can be interpreted as electronic charge placed in a π orbital on the PTCDA molecule, which is then screened by the metal. This leads to charge oscillations in the metal substrate, similar to what is observed in graphene adsorbed on metals,[110] which resemble Friedel oscillations.

Adsorption of PTCDA on Au is qualitatively different from adsorption on the other metal surfaces, as can be judged from the signs of the interface dipoles and the charges. The charge distribution of PTCDA on Au, Fig. 11(c), is also qualitatively different. It is more localized in the region between the molecule and the surface, as can be expected if it is due to Pauli repulsion (i.e., the pillow effect), since the latter is active in the region where the molecular and the surface wave functions overlap.

Since this overlap decreases with increasing distance between the molecule and the surface, one expects the charge displacement to decrease accordingly. Indeed the charge on PTCDA adsorbed on Au, calculated using Eq. (11), at a distance $d=3.6$ Å is $0.23e$, as compared to $0.34e$ at $d=3.0$ Å, see Table V. The pillow effect is a very general mechanism that should be operative for any adsorbed closed-shell molecule, even if electrons are transferred from the substrate to the LUMO, as for PTCDA adsorbed on other metal surfaces. One would expect that this leads to an interface dipole that depends strongly on the molecule-surface distance. However, Fig. 5 shows that for PTCDA on Ag and Al (and to a lesser extend also for PTCDA on Mg), the work function, and therefore the interface dipole, is independent of the distance over a considerable range.

C. Model

In this section we aim at setting up a simple model that explains qualitatively the most prominent features of the

work functions of molecular monolayers adsorbed on metal surfaces. In particular, we want to identify the different regimes, i.e., work function decrease by the pillow effect and work-function pinning by charge transfer. Moreover, the lack of the work-function dependence on the molecule surface distance in the pinning regime should be clarified.

To construct this model we assume that the relevant energy scale is set by molecular properties such as the HOMO-LUMO gap, and neglect the broadening of molecular levels introduced by the interaction between the molecule and the surface. We assume that electrons can be transferred to a molecular level, whose energy $\epsilon_M(N)$ depends on the occupation number N, as in Eq. (6). In the spirit of Slater's transition state approach N can take any value $0 \leq N \leq 2$.[143] The charging energy U depends on the environment of the molecule. All molecules in a monolayer have the same occupation number and in the effective U the interactions between all molecules should be taken into account, as well as the interactions with the metal substrate.

If the molecular layer is in equilibrium with the metal substrate, one has $\epsilon_M(N) = E_F$, with E_F the Fermi level of the metal. This determines the occupation number

$$N = \frac{E_F - \epsilon_0}{U}. \tag{12}$$

Obviously this expression is valid only if $0 \leq N \leq 2$. The idea is illustrated by Fig. 12(b). To simplify the description we discuss electron transfer to the LUMO, but the resulting expressions are easily generalized, see below.

If $N > 0$, the molecular layer is charged and with the screening charge in the metal substrate this leads to a dipole layer. It results in a potential step at the interface, which we parameterize as NF with F the potential step normalized per electron transferred to a molecule. The work function then becomes

$$W = W_c + NF \tag{13}$$

with $W_c = -E_F$ the work function of the clean metal surface.

So far we have not yet taken the pillow effect into account, which lowers the work function of the clean metal surface from W_c to $W_c - \Delta$. As discussed in the previous section, the pillow effect leads to an interface dipole that is localized mainly between the surface and the molecule, see Fig. 11(c). Therefore, it is consistent to apply the potential step to the molecular levels and replace ϵ_0 by $\epsilon_0 - \Delta$ in Eq. (12). The idea is illustrated by Fig. 12(a). Replacing W_c with $W_c - \Delta$ in Eq. (13) and using Eq. (12) then gives

$$W = (W_c - \Delta)\left(1 - \frac{F}{U}\right) - \epsilon_0 \frac{F}{U}. \tag{14}$$

The S parameter, Eq. (1), is then given by

$$S = 1 - \frac{F}{U}. \tag{15}$$

From purely electrostatic considerations one has $0 < F \leq U$,[141] and $0 \leq S \leq 1$.

Since $0 \leq N \leq 2$, Eqs. (14) and (15) are valid if $\Delta - \epsilon_0 - 2U \leq W_c \leq \Delta - \epsilon_0$. If the clean metal work function is too large, $W_c > \Delta - \epsilon_0$, there is no electron transfer and the molecular level is unoccupied $N = 0$. Only the pillow effect is then operative and the work function is unpinned

$$W = W_c - \Delta; \quad S = 1. \tag{16}$$

If the clean metal work function is too small, $W_c < \Delta - \epsilon_0 - 2U$, the molecular level is fully occupied with $N = 2$. The work function is again unpinned, but is now given by the expression

$$W = W_c - \Delta + 2F; \quad S = 1. \tag{17}$$

Figure 12(c) summarizes these relations. In principle the clean metal work function can be decreased further on the left side of this figure, so that the next molecular level (LUMO+1) gets partially occupied. This again pins the work function and adds a plateau on the left side of this figure, described by replacing $W_c - \Delta$ by $W_c - \Delta + 2F$ in Eq. (14) (and ϵ_0 representing the LUMO+1 level). Upon increas-

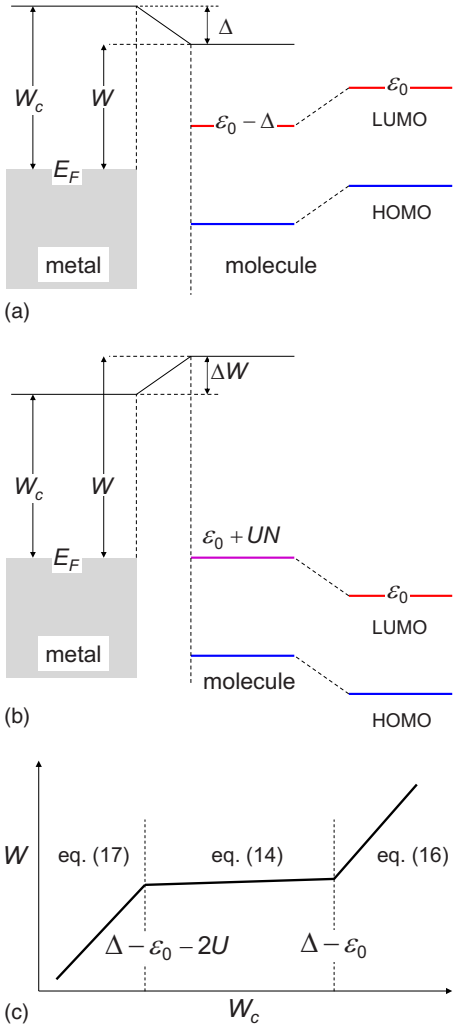

FIG. 12. (Color online) (a) The pillow effect results in a potential step Δ, which lowers the molecular levels close to the interface. (b) Charge transfer to the LUMO raises the molecular levels and pins the Fermi level. (c) The work function W as function of the clean metal work function W_c according to Eqs. (14)–(17).

ing the clean metal work function on the right side of the figure, electron transfer from the molecule to the metal can take place, which partially depopulates the HOMO. This again pins the work function and adds a plateau on the left side of the diagram, described by Eq. (14) with ϵ_0 representing the HOMO level.

The expressions of Eqs. (14) and (15) can be simplified considerably if charge on the molecular layer and its counter charge in the metal substrate can be modeled by a plane capacitor. In that case we have $U=F=e^2/C$, where C is the "capacitance" of the molecule,[130,141] which leads to the simple expressions

$$W=-\epsilon_0; \quad S=0. \tag{18}$$

In this limit one has perfect pinning, i.e., the work function is determined by the molecular level only. It is independent of the metal and of the pillow effect.

This simple model can be used to qualitatively describe the work functions in Figs. 4–7. The simplest case is if $W_c > \Delta-\epsilon_0$, i.e., if the work functions of all the metals considered are too high with respect to the position of the LUMO level. W and S are then given by Eq. (16), i.e., the work function is simply shifted with respect to the work function of the clean metal surface. Benzene adsorbed on metal surfaces is such a case, see Fig. 6. Since the work-function shift is determined by the pillow effect, one expects it to be sensitive the distance between the molecule and the surface, which can be observed in Fig. 6.

If $W_c \leq \Delta-\epsilon_0$, the LUMO reaches the Fermi level of the metal. W and S are given by Eq. (14), and in the simple plane capacitor model by Eq. (18). A close-packed monolayer of planar molecules, such as in the herringbone structure of PTCDA [Fig. 1(b)], comes closest to a plane capacitor. Figure 5 shows that indeed the work function is pinned at ~4.7 eV over a considerable range of metal work functions and molecule-surface distances. If $W_c < \Delta-\epsilon_0-2U$, the LUMO becomes fully occupied. W and S are given by Eq. (17) and the work function becomes unpinned.

The energy at which this occurs depends on the molecule-surface distance. Decreasing the distance increases the pillow effect, i.e., it increases Δ. Moreover it decreases U, since at a shorter distance the screening by the metal substrate is larger. In the plane capacitor model $U \propto 1/d$, where d is the molecule-surface distance. The distance dependence of the unpinning of the work function is observed in Fig. 5. At $d=3.6$ Å the work function is fully pinned, at $d=3.3$ Å it becomes unpinned for Ca, and at $d=3.0$ Å it is unpinned for Ca and Mg.

The dilute structure for PTCDA has only $\sim\frac{1}{2}$ ML coverage [Fig. 1(a)]. This situation cannot be described by a simple plane capacitor, and one has to use Eq. (14). It gives a linear dependence of W on W_c with a slope $0<S<1$, which can be observed in Fig. 4.

The behavior of perylene is consistent with the model given above. If $W_c > \Delta-\epsilon_0$, only the pillow effect is operative and the LUMO is unoccupied, cf. Eq. (16). This holds for Au and Ag in Figs. 7(a) and 7(b). If $W_c \leq \Delta-\epsilon_0$, we observe pinning. For a close-packed monolayer the plane capacitor model explains the pinning [Eq. (18)] observed for Mg and Ca in Fig. 7(b). For the dilute structure with $\sim\frac{1}{2}$ ML packing density, Eq. (14) can be used to describe the behavior for adsorption on the low-work-function metals.

VI. SUMMARY AND CONCLUSIONS

We study the interface dipole formation at interfaces formed by a monolayers of PTCDA, benzene, and perylene molecules with the Au, Ag, Al, and Ca(111) and the Mg(0001) surfaces, using first-principles DFT calculations. The interface dipoles are monitored by calculating the change in the surface work function upon adsorption of the molecular layer. Molecular packing densities corresponding to $\frac{1}{2}$ ML and 1 ML coverage are considered and the distance between the molecules and the surfaces is varied to establish the dependence of the work function on these parameters.

Adsorption of PTCDA in a densely pack structure leads to pinning ($S=0$) of the work function at ~4.7 eV for a range of metal substrates and molecule-substrate distances, in good agreement with experimental observations. The interface dipoles that are created upon adsorption compensate for the differences between the work functions of the different clean metal surfaces. Along the series Ag, Al, Mg, and Ca the interface dipole generated by PTCDA adsorption increases, which is consistent with an increasing transfer of electrons from the substrate to the PTCDA molecules. The increased electron transfer also leads to a stronger bond between the molecule and the surface. Decreasing the packing density of the PTCDA molecules to $\frac{1}{2}$ ML decreases the pinning effect, but it still gives a linear dependence between the work function of the adsorbed layer and that of the clean metal surfaces ($S \approx 0.5$). Adsorption of PTCDA on Au(111) leads to a very weak bond and an interface dipole that has an opposite sign, as compared to the other surfaces. Here the pillow effect is dominant, which pushes the electrons into the metal substrate.

Adsorption of benzene results in a reduction of the work function, irrespective of the substrate, in agreement with experiments. This reduction is in the range 0.2–0.8 eV, depending on the distance between the molecule and the surface. At a fixed distance $S \approx 0.9$. In the case of benzene adsorption only the pillow effect is operative. The latter, as well as the effect of charge transfer to the molecule are observed in adsorption of perylene. Adsorption of a full ML of perylene molecules on low-work-function metals gives work-function pinning ($S=0$) at ~3.7 eV. Adsorption on high-work-function metals gives the work-function reduction characteristic of the pillow effect with $S \approx 0.9$. The transition between the two regimes takes place for substrate work functions in the range Mg-Al. Decreasing the packing density decreases the pinning in the low-work-function regime.

A simple model inspired by Slater's transition state approach allows us to describe the changes in the work function upon adsorption qualitatively. The model incorporates the charge transfer between the substrate and the molecular levels, the charging energy of the molecules, the pillow effect, and the interface dipole layer. It shows that for planar molecules the work function is pinned at a level that is determined by the molecules and not by the substrate. That

level does not correspond to the molecular EA, but lies within the transport gap of the molecular material.

ACKNOWLEDGMENTS

The authors thank Menno Bokdam for his help in completing the paper. This work is part of the research programs of the Stichting voor Fundamenteel Onderzoek der Materie (FOM), financially supported by the Nederlandse Organisatie voor Wetenschappelijk Onderzoek (NWO), and of NanoNed, a nanotechnology program of the Dutch Ministry of Economic Affairs. The use of supercomputer facilities was sponsored by the Stichting Nationale Computer Faciliteiten (NCF), financially supported by NWO.

[1] C. W. Tang and S. A. VanSlyke, Appl. Phys. Lett. **51**, 913 (1987).
[2] J. H. Burroughes, D. D. C. Bradley, A. R. Brown, R. N. Marks, K. Mackay, R. H. Friend, P. L. Burns, and A. B. Holmes, Nature (London) **347**, 539 (1990).
[3] A. Tsumura, H. Koezuka, and T. Ando, Appl. Phys. Lett. **49**, 1210 (1986).
[4] F. Garnier, R. Hajlaoui, A. Yassar, and P. Srivastava, Science **265**, 1684 (1994).
[5] N. S. Sariciftci, L. Smilowitz, A. J. Heeger, and F. Wudl, Science **258**, 1474 (1992).
[6] G. Yu, J. Wang, J. McElvain, and A. J. Heeger, Adv. Mater. **10**, 1431 (1998).
[7] M. E. Gershenson, V. Podzorov, and A. F. Morpurgo, Rev. Mod. Phys. **78**, 973 (2006).
[8] A. Kahn, N. Koch, and W. Gao, J. Polym. Sci., Part B: Polym. Phys. **41**, 2529 (2003).
[9] G. Brocks, Synth. Met. **102**, 914 (1999).
[10] G. Brocks, J. van den Brink, and A. F. Morpurgo, Phys. Rev. Lett. **93**, 146405 (2004).
[11] G. Giovannetti, G. Brocks, and J. van den Brink, Phys. Rev. B **77**, 035133 (2008).
[12] M. F. Craciun, G. Giovannetti, S. Rogge, G. Brocks, A. F. Morpurgo, and J. van den Brink, Phys. Rev. B **79**, 125116 (2009).
[13] I. N. Hulea, S. Russo, A. Molinari, and A. F. Morpurgo, Appl. Phys. Lett. **88**, 113512 (2006).
[14] R. T. Tung, Phys. Rev. Lett. **84**, 6078 (2000).
[15] R. T. Tung, Phys. Rev. B **64**, 205310 (2001).
[16] P. C. Rusu and G. Brocks, Phys. Rev. B **74**, 073414 (2006).
[17] V. De Renzi, R. Rousseau, D. Marchetto, R. Biagi, S. Scandolo, and U. del Pennino, Phys. Rev. Lett. **95**, 046804 (2005).
[18] G. Heimel, L. Romaner, J.-L. Brédas, and E. Zojer, Phys. Rev. Lett. **96**, 196806 (2006).
[19] P. C. Rusu and G. Brocks, J. Phys. Chem. B **110**, 22628 (2006).
[20] G. Heimel, L. Romaner, E. Zojer, and J.-L. Brédas, Nano Lett. **7**, 932 (2007).
[21] P. C. Rusu, G. Giovannetti, and G. Brocks, J. Phys. Chem. C **111**, 14448 (2007).
[22] I. G. Hill, A. Rajagopal, and A. Kahn, Appl. Phys. Lett. **73**, 662 (1998).
[23] H. Ishii, K. Sugiyama, E. Ito, and K. Seki, Adv. Mater. **11**, 605 (1999).
[24] N. Koch, S. Duhm, J. P. Rabe, A. Vollmer, and R. L. Johnson, Phys. Rev. Lett. **95**, 237601 (2005).
[25] M. Knupfer and T. Schwieger, Appl. Surf. Sci. **252**, 77 (2005).
[26] H. Ishii, N. Hayashi, E. Ito, Y. Washizu, K. Sugi, Y. Kimura, M. Niwano, Y. Ouchi, and K. Seki, Phys. Status Solidi A **201**, 1075 (2004).
[27] V. Heine, Phys. Rev. **138**, A1689 (1965).
[28] S. G. Louie, J. R. Chelikowsky, and M. L. Cohen, Phys. Rev. B **15**, 2154 (1977).
[29] C. Tejedor, F. Flores, and E. Louis, J. Phys. C **10**, 2163 (1977).
[30] H. Vázquez, R. Oszwaldowski, P. Pou, J. Ortega, R. Pérez, F. Flores, and A. Kahn, Europhys. Lett. **65**, 802 (2004).
[31] H. Vázquez, F. Flores, R. Oszwaldowski, J. Ortega, R. Pérez, and A. Kahn, Appl. Surf. Sci. **234**, 107 (2004).
[32] H. Vázquez, Y. J. Dappe, J. Ortega, and F. Flores, J. Chem. Phys. **126**, 144703 (2007).
[33] J. L. F. D. Silva, C. Stampfl, and M. Scheffler, Phys. Rev. Lett. **90**, 066104 (2003).
[34] P. S. Bagus, V. Staemmler, and C. Wöll, Phys. Rev. Lett. **89**, 096104 (2002).
[35] X. Crispin, V. Geskin, A. Crispin, J. Cornil, R. Lazzaroni, W. R. Salaneck, and J.-L. Bredas, J. Am. Chem. Soc. **124**, 8131 (2002).
[36] Y. Morikawa, H. Ishii, and K. Seki, Phys. Rev. B **69**, 041403(R) (2004).
[37] G. Witte, S. Lukas, P. S. Bagus, and C. Wöll, Appl. Phys. Lett. **87**, 263502 (2005).
[38] Y. C. Chen, J. E. Cunningham, and C. P. Flynn, Phys. Rev. B **30**, 7317 (1984).
[39] J. Tang, C. Lee, S. Lee, and Y. Xu, Chem. Phys. Lett. **396**, 92 (2004).
[40] C. Tengstedt, W. Osikowicz, W. R. Salaneck, I. D. Parker, C.-H. Hsu, and M. Fahlman, Appl. Phys. Lett. **88**, 053502 (2006).
[41] N. Koch and A. Vollmer, Appl. Phys. Lett. **89**, 162107 (2006).
[42] N. Koch, ChemPhysChem **8**, 1438 (2007).
[43] M. Fahlman, A. Crispin, X. Crispin, S. K. M. Henze, M. P. de Jong, W. Osikowicz, C. Tengstedt, and W. R. Salaneck, J. Phys.: Condens. Matter **19**, 183202 (2007).
[44] S. Braun, W. R. Salaneck, and M. Fahlman, Adv. Mater. **21**, 1450 (2009).
[45] P. S. Davids, A. Saxena, and D. L. Smith, J. Appl. Phys. **78**, 4244 (1995).
[46] P. C. Rusu, G. Giovannetti, C. Weijtens, R. Coehoorn, and G. Brocks, J. Phys. Chem. C **113**, 9974 (2009).
[47] S. R. Forrest, Chem. Rev. **97**, 1793 (1997).
[48] E. Umbach, K. Glöckler, and M. Sokolowski, Surf. Sci. **402-404**, 20 (1998).
[49] M. Eremtchenko, J. A. Schaefer, and F. S. Tautz, Nature (London) **425**, 602 (2003).
[50] M. Eremtchenko, D. Bauer, J. A. Schaefer, and F. S. Tautz, New J. Phys. **6**, 4 (2004).
[51] A. Hauschild, K. Karki, B. C. C. Cowie, M. Rohlfing, F. S. Tautz, and M. Sokolowski, Phys. Rev. Lett. **94**, 036106 (2005).
[52] Y. Zou, L. Kilian, A. Schöll, T. Schmidt, R. Fink, and E. Um-

bach, Surf. Sci. **600**, 1240 (2006).
[53] A. Kraft, R. Temirov, S. K. M. Henze, S. Soubatch, M. Rohlfing, and F. S. Tautz, Phys. Rev. B **74**, 041402(R) (2006).
[54] R. Temirov, S. Soubatch, A. Luican, and F. S. Tautz, Nature (London) **444**, 350 (2006).
[55] A. Gerlach, S. Sellner, F. Schreiber, N. Koch, and J. Zegenhagen, Phys. Rev. B **75**, 045401 (2007).
[56] L. Romaner, D. Nabok, P. Puschnig, E. Zojer, and C. Ambrosch-Draxl, New J. Phys. **11**, 053010 (2009).
[57] S. Duhm, A. Gerlach, I. Salzman, B. Bröker, R. L. Johnson, F. Schreiber, and N. Koch, Org. Electron. **9**, 111 (2008).
[58] E. Kawabe, H. Yamane, R. Sumii, K. Koizumi, and Y. Ouchi, Org. Electron. **9**, 783 (2008).
[59] R. Dudde, K.-H. Frank, and E.-E. Koch, Surf. Sci. **225**, 267 (1990).
[60] X.-L. Zhou, M. Castro, and J. White, Surf. Sci. **238**, 215 (1990).
[61] D. Velic, A. Hotzel, M. Wolf, and G. Ertl, J. Chem. Phys. **109**, 9155 (1998).
[62] R. Duschek, F. Mittendorfer, R. Blyth, F. Netzer, J. Hafner, and M. Ramsey, Chem. Phys. Lett. **318**, 43 (2000).
[63] K. Gaffney, C. Wong, S. Liu, A. Miller, J. McNeill, and C. Harris, Chem. Phys. **251**, 99 (2000).
[64] C. Seidel, R. Ellerbrake, L. Gross, and H. Fuchs, Phys. Rev. B **64**, 195418 (2001).
[65] M. Eremtchenko, D. Bauer, J. Schaefer, and F. Tautz, J. Mater. Res. **19**, 2028 (2004).
[66] L. Yan, N. J. Watkins, S. Zorba, Y. Gao, and C. W. Tang, Appl. Phys. Lett. **81**, 2752 (2002).
[67] P. Hohenberg and W. Kohn, Phys. Rev. **136**, B864 (1964).
[68] W. Kohn and L. J. Sham, Phys. Rev. **140**, A1133 (1965).
[69] J. P. Perdew and A. Zunger, Phys. Rev. B **23**, 5048 (1981).
[70] D. M. Ceperley and B. J. Alder, Phys. Rev. Lett. **45**, 566 (1980).
[71] J. P. Perdew, J. A. Chevary, S. H. Vosko, K. A. Jackson, M. R. Pederson, D. J. Singh, and C. Fiolhais, Phys. Rev. B **46**, 6671 (1992).
[72] G. Kresse and J. Hafner, Phys. Rev. B **47**, 558 (1993).
[73] G. Kresse and J. Furthmüller, Phys. Rev. B **54**, 11169 (1996).
[74] G. Kresse and D. Joubert, Phys. Rev. B **59**, 1758 (1999).
[75] P. E. Blöchl, Phys. Rev. B **50**, 17953 (1994).
[76] J. Neugebauer and M. Scheffler, Phys. Rev. B **46**, 16067 (1992).
[77] H. J. Monkhorst and J. D. Pack, Phys. Rev. B **13**, 5188 (1976).
[78] M. Methfessel and A. T. Paxton, Phys. Rev. B **40**, 3616 (1989).
[79] P. E. Blöchl, O. Jepsen, and O. K. Andersen, Phys. Rev. B **49**, 16223 (1994).
[80] C. J. Fall, N. Binggeli, and A. Baldereschi, J. Phys.: Condens. Matter **11**, 2689 (1999).
[81] M. W. Schmidt, K. K. Baldridge, J. A. Boatz, S. T. Elbert, M. S. Gordon, J. J. Jensen, S. Koseki, N. Matsunaga, K. A. Nguyen, S. Su, T. L. Windus, M. Dupuis, and J. A. Montgomery, Jr., J. Comput. Chem. **14**, 1347 (1993).
[82] A. D. Becke, Phys. Rev. A **38**, 3098 (1988).
[83] C. Lee, W. Yang, and R. G. Parr, Phys. Rev. B **37**, 785 (1988).
[84] A. Modelli, L. Mussoni, and D. Fabbri, J. Phys. Chem. A **110**, 6482 (2006).
[85] M. Andrzejak, G. Mazur, and P. Petelenz, J. Mol. Struct.: THEOCHEM **527**, 91 (2000).
[86] G. V. Hansson and S. A. Flodstrom, Phys. Rev. B **18**, 1572 (1978).
[87] M. Chelvayohan and C. H. B. Mee, J. Phys. C **15**, 2305 (1982).
[88] R. C. Monreal, L. Guillemot, and V. A. Esaulov, J. Phys.: Condens. Matter **15**, 1165 (2003).
[89] K. Giesen, F. Hage, F. J. Himpsel, H. J. Riess, W. Steinmann, and N. V. Smith, Phys. Rev. B **35**, 975 (1987).
[90] J. K. Grepstad, P. O. Gartland, and B. J. Slagsvold, Surf. Sci. **57**, 348 (1976).
[91] P. A. Anderson, Phys. Rev. **54**, 753 (1938).
[92] H. B. Michaelson, J. Appl. Phys. **48**, 4729 (1977).
[93] S. Piccinin, A. Selloni, S. Scandolo, R. Car, and G. Scoles, J. Chem. Phys. **119**, 6729 (2003).
[94] M. L. Bocquet, A. M. Rappe, and H. L. Dai, Mol. Phys. **103**, 883 (2005).
[95] A. Curioni and W. Andreoni, IBM J. Res. Dev. **45**, 101 (2001).
[96] E. Wachowicz and A. Kiejna, J. Phys.: Condens. Matter **13**, 10767 (2001).
[97] H. L. Skriver and N. M. Rosengaard, Phys. Rev. B **46**, 7157 (1992).
[98] T. Schmitz-Hübsch, T. Fritz, F. Sellam, R. Staub, and K. Leo, Phys. Rev. B **55**, 7972 (1997).
[99] P. Fenter, F. Schreiber, L. Zhou, P. Eisenberger, and S. R. Forrest, Phys. Rev. B **56**, 3046 (1997).
[100] N. Nicoara, E. Román, J. M. Gómez-Rodríguez, J. A. Martín-Gago, and J. Méndez, Org. Electron. **7**, 287 (2006).
[101] B. Krause, A. C. Dürr, F. Schreiber, and H. Dosch, J. Chem. Phys. **119**, 3429 (2003).
[102] S. X. Du, H. J. Gao, C. Seidel, L. Tsetseris, W. Ji, H. Kopf, L. F. Chi, H. Fuchs, S. J. Pennycook, and S. T. Pantelides, Phys. Rev. Lett. **97**, 156105 (2006).
[103] Y. Hirose, A. Kahn, V. Aristov, P. Soukiassian, V. Bulovic, and S. R. Forrest, Phys. Rev. B **54**, 13748 (1996).
[104] S. Kera, H. Setoyama, M. Onoue, K. K. Okudaira, Y. Harada, and N. Ueno, Phys. Rev. B **63**, 115204 (2001).
[105] T. Kampen, A. Das, S. Park, W. Hoyer, and D. Zahn, Appl. Surf. Sci. **234**, 333 (2004).
[106] G. Gavrila, D. R. T. Zahn, and W. Braun, Appl. Phys. Lett. **89**, 162102 (2006).
[107] G. G. Fuentes and M. Knupfer, Appl. Phys. A: Mater. Sci. Process. **84**, 329 (2006).
[108] S. Picozzi, A. Pecchia, M. Gheorghe, A. Di Carlo, P. Lugli, B. Delley, and M. Elstner, Phys. Rev. B **68**, 195309 (2003).
[109] G. Giovannetti, P. A. Khomyakov, G. Brocks, V. M. Karpan, J. van den Brink, and P. J. Kelly, Phys. Rev. Lett. **101**, 026803 (2008).
[110] P. A. Khomyakov, G. Giovannetti, P. C. Rusu, G. Brocks, J. van den Brink, and P. J. Kelly, Phys. Rev. B **79**, 195425 (2009).
[111] K. Lee, J. Yu, and Y. Morikawa, Phys. Rev. B **75**, 045402 (2007).
[112] R. Rurali, N. Lorente, and P. Ordejo'n, Phys. Rev. Lett. **95**, 209601 (2005).
[113] A. Hauschild, K. Karki, B. C. C. Cowie, M. Rohlfing, F. S. Tautz, and M. Sokolowski, Phys. Rev. Lett. **95**, 209602 (2005).
[114] H. Rydberg, M. Dion, N. Jacobson, E. Schroder, P. Hyldgaard, S. I. Simak, D. C. Langreth, and B. I. Lundqvist, Phys. Rev. Lett. **91**, 126402 (2003).
[115] T. Thonhauser, V. R. Cooper, S. Li, A. Puzder, P. Hyldgaard, and D. C. Langreth, Phys. Rev. B **76**, 125112 (2007).
[116] M. Vanin, J. J. Mortensen, A. K. Kelkkanen, J. M. Garcia-Lastra, K. S. Thygesen, and K. W. Jacobsen, Phys. Rev. B **81**, 081408 (2010).
[117] M. Rohlfing and T. Bredow, Phys. Rev. Lett. **101**, 266106 (2008).

[118] L. Romaner, G. Heimel, J.-L. Brédas, A. Gerlach, F. Schreiber, R. L. Johnson, J. Zegenhagen, S. Duhm, N. Koch, and E. Zojer, Phys. Rev. Lett. **99**, 256801 (2007).
[119] G. M. Rangger, O. T. Hofmann, L. Romaner, G. Heimel, B. Bröker, R.-P. Blum, R. L. Johnson, N. Koch, and E. Zojer, Phys. Rev. B **79**, 165306 (2009).
[120] G. Brocks, Phys. Rev. B **55**, 6816 (1997).
[121] H. Vázquez, Ph.D. thesis, Universidad Autonoma de Madrid, 2006.
[122] N. Dori, M. Menon, L. Kilian, M. Sokolowski, L. Kronik, and E. Umbach, Phys. Rev. B **73**, 195208 (2006).
[123] D. P. Chong, O. V. Gritsenko, and E. J. Baerends, J. Chem. Phys. **116**, 1760 (2002).
[124] O. V. Gritsenko, B. Braïda, and E. J. Baerends, J. Chem. Phys. **119**, 1937 (2003).
[125] M. Grüning, O. V. Gritsenko, S. J. A. van Gisbergen, and E. J. Baerends, J. Chem. Phys. **116**, 9591 (2002).
[126] Y. M. Niquet and X. Gonze, Phys. Rev. B **70**, 245115 (2004).
[127] M. Grüning, A. Marini, and A. Rubio, J. Chem. Phys. **124**, 154108 (2006).
[128] J. C. Slater, *The Self-Consistent Field for Molecules and Solids* (McGraw-Hill, New York, 1974).
[129] J. F. Janak, Phys. Rev. B **18**, 7165 (1978).
[130] J. R. Sabin, S. B. Trickey, S. P. Apell, and J. Oddershede, Int. J. Quantum Chem. **77**, 358 (2000).
[131] Note that the total energy of a molecular ion with N additional electrons, can be written as $E_{\mathrm{tot}}(N)=E_{\mathrm{tot}}(0)+\epsilon_0 N+\frac{1}{2}UN^2$.
[132] E. V. Tsiper, Z. G. Soos, W. Gao, and A. Kahn, Chem. Phys. Lett. **360**, 47 (2002).
[133] The factor 2 originates from writing the total energy of a molecular ion with N additional electrons, embedded in a crystal, as $E_{\mathrm{tot}}(N)=E_{\mathrm{tot}}(0)+\epsilon_0 N+\frac{1}{2}U_{\mathrm{bare}}N^2-P^{N-}$. If the polarization energy P^{N-} is determined purely by electrostatics, then $P^{N-}=N^2P^{-}$. Writing the total energy as in Ref. 131 then leads to Eq. (8).
[134] I. Hill, A. Kahn, Z. Soos, and J. R. A. Pascal, Chem. Phys. Lett. **327**, 181 (2000).
[135] A. Zangwill, *Physics at Surfaces* (Cambridge University Press, Cambridge, 1988).
[136] J. Kröger, H. Jensen, R. Berndt, R. Rurali, and N. Lorente, Chem. Phys. Lett. **438**, 249 (2007).
[137] J. Tersoff, Phys. Rev. Lett. **52**, 465 (1984).
[138] J. Tersoff, Phys. Rev. B **32**, 6968 (1985).
[139] S. G. Louie and M. L. Cohen, Phys. Rev. B **13**, 2461 (1976).
[140] N. D. Lang and A. R. Williams, Phys. Rev. B **18**, 616 (1978).
[141] J. D. Jackson, *Classical Electrodynamics* (Wiley, New York, 1975).
[142] Any scheme to divide a charge distribution over subsystems has an element of arbitrariness. Consequently the absolute numbers obtained for (partial) charges differ from scheme to scheme. The relative numbers obtained for different, but similar, systems, however, give a good indication of the trend. The scheme we use here follows naturally from the charge-density difference.
[143] In the integer charge-transfer (ICT) model, N is restricted to an integer (Refs. 43 and 44). In that case one needs to invoke a mixture of charged and uncharged molecules to interpret work-function pinning, Ref. 45, which may lead to a nonuniformly charged organic layer. The ICT model is developed for organic layers that are separated from the metal by a tunnel barrier. In the cases discussed in this paper, the organic layer is in close contact with the metal and partial occupations can be achieved by hybridization of the molecular and the metal states.